第 43 卷 第 3 期/2023 年 2 月/光学学报 研究论文

光学学报

微米级双层复合结构的一步光刻制备技术

张登英[1,2,3,4*]，朱林伟[3]，李伟任[3]，高鸿鹄[3]，邢文强[3]，姜潇桐[3]，王军[2]，徐征[1,4**]

[1]北京交通大学光电子技术研究所，北京 100044；

[2]北京太阳能电力研究院有限公司，北京 101102；

[3]鲁东大学物理与光电工程学院，山东 烟台 264025；

[4]北京交通大学发光与光信息技术教育部重点实验室，北京 100044

摘要 设计了两种具有不同参数的光刻掩模版，利用光刻技术制备了两种微米级双层复合结构。研究了曝光能量对凹形缺口深度的影响，同时采用有限差分时域法分析了掩模版曝光时的光场分布情况，阐明了微米级双层复合结构形成的物理机理。实验结果表明：通过调整曝光能量的大小，能够有效地控制凹形缺口的深度。对 8 μm 厚的 AZ9260 光刻胶来说，不高于 160 mJ/cm^2 的曝光能量是制备出微米级双层复合结构的关键。该技术在制备微米尺寸的分层器件方面有着潜在的应用前景。

关键词 光学器件；微结构制造；光刻；微米级双层复合结构；有限差分时域法

中图分类号 O436 **文献标志码** A **DOI**：10.3788/AOS221414

1 引 言

自然界中具有特殊微结构的生物体表面往往能够展现出令人赞叹的优异性能。例如，常见的荷叶表面具有超疏水和自清洁的性能[1]、蚊子的复眼具有超疏水防雾的性能[2]、鲨鱼的皮具有减少阻力的性能[3-4]和壁虎的脚具有超级黏附的性能[5]等。师法自然一直是人类科技进步的一个重要思想源泉，设计并构建出这些奇特的仿生微结构表面为人类所用是近年来国内外的一个研究热点。当前，人工构建的微结构已经被广泛应用于光电子器件[6]、生物医学[7]、柔性电子器件[8]、各类传感器[8-10]和组织工程[11-12]等领域中。因此，微结构加工方法也得到了发展，如干法/湿法刻蚀[6]、纳米压印[7-8]、3D 打印[9-12]、自组装[10, 13]、激光加工[14-15]、光刻[13, 16-22]、复制模塑[13, 16]和静电纺丝[17]等。利用这些技术的组合往往可以制备出各种各样的单层微结构表面，甚至可以制备出多尺度的微-微复合结构表面和微-纳复合结构表面。

多尺度的微-微复合结构和微-纳复合结构能够表现出比单层结构更加优异的机械性能、光学性能和化学性能，故得到了研究人员的广泛关注。Wang 等[13]利用光刻、自组装和复制模塑技术制备了仿生复眼结构，获得了数值孔径达到 0.77 的单个小眼，使光学成像更加清晰。王成[16]和 Chen 等[17]利用光刻、复制模塑和静电纺丝等技术制备出了各种微-微复合结构和微-纳复合结构，构建出了能够获取机械能和水能的高性能摩擦纳米发电机。Lü 等[18]利用光刻、化学刻蚀和复制模塑等技术在形状记忆聚合物上制备了微纳米结构阵列，获得了一种具有形状记忆能力的超疏水表面，并将其成功地应用于可重写的液滴存储功能芯片中，解决了图案无法被重新编程的难题。

毫无疑问，利用传统光刻技术来制备微米结构时非常便捷且操作简单。然而，在利用光刻技术制备微-微复合结构时以往都需要使用套刻工艺并经过多次光刻才能够实现，而套刻工艺的使用极大地增加了微结构的加工成本和制作难度。本文介绍了一种通过改变掩模版上透光部分的宽窄来调节光刻胶曝光效率的方法，利用该方法仅需一次曝光即可在正性光刻胶上获得微-微复合结构，可以用于微米级多通道结构的制备研究[23]。所提方法极大地降低了微-微复合结构的加工难度，并为制备多尺度复合结构提供了一种新的策略。同时，本文还利用有限差分时域法对掩模版透光结构进行了光学仿真，阐明了微-微复合结构能够通过一步光刻成形的内在机理。

2 样品制备和表征

本文使用的是从中国电子科技集团第五十五研究所订制的在普通玻璃表面镀 Cr 膜的掩模版，掩模版上

收稿日期：2022-07-04；**修回日期**：2022-08-04；**录用日期**：2022-08-12；**网络首发日期**：2022-08-22

基金项目：国家自然科学基金(61705096，62174073)、中国博士后基金(2018M631385)

通信作者：*zhangdengying@ldu.edu.cn；**zhengxu@bjtu.edu.cn

的图案结构尺寸是所提技术能够成功应用的关键。本实验所使用的掩模版上的图案结构分布和参数如图 1 所示。掩模版图案由周期性条带结构组成，图中空白的部分为透光区域，填充的部分为不透光区域。1 号掩模版上条带结构一个周期的总宽度为 80 μm，一个周期内透光区域的宽度分别为 4 μm 和 40 μm，不透光区域宽度均为 18 μm。2 号掩模版上条带结构一个周期的总宽度为 120μm，透光区域的宽度分别为 4、4、60 μm，不透光区域宽度均为 17.33 μm。

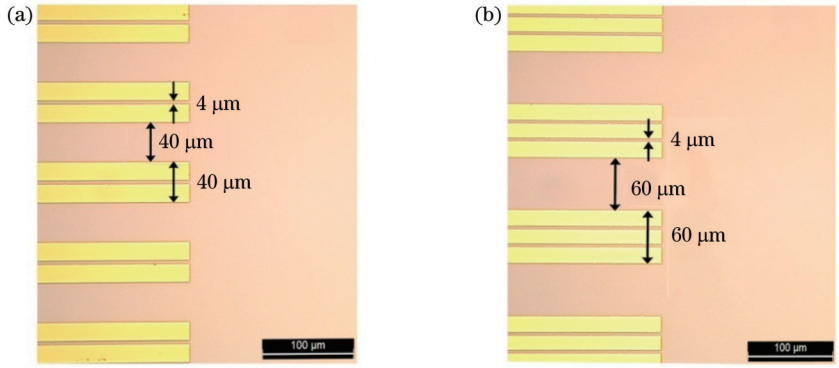

图 1 掩模版布局示意图。(a) 1 号掩模版；(b) 2 号掩模版

Fig. 1 Layout diagram of masks. (a) Mask 1; (b) mask 2

实验采用的光刻胶是 AZ9260 正性光刻胶，使用的基片是直径为 5.08 cm、厚度为 0.5 mm 的 K_9 玻璃片。本实验的一步光刻工艺如图 2 所示，以 1 号掩模版为例，具体的实验工艺为：1)基片清洗，将 K_9 玻璃片基底依次置于丙酮、乙醇和去离子水中超声清洗 5 min，清洗干净后使用氮气吹干；2)匀胶，使用 Laurell WS-650Mz 匀胶机将 AZ9260 光刻胶旋涂在干净的 K_9 基片上，设置匀胶机的高速转速为 2500 r/min，在此转速下匀胶 40 s，可在 K_9 基片上得到厚度为 8 μm 的光刻胶涂层；3)烘胶，将匀胶后的基片先在室温下静置 10 min，再将该基片依次置于 65 ℃热板、95 ℃热板、110 ℃热板上加热 5、10、5 min，最后冷却至室温；4)紫外(UV)曝光，使用 Midas MDA-400M 光刻机和图 1 中的掩模版进行 UV 曝光，不同样品的曝光能量设定在 125～240 mJ/cm^2 之间；5)显影，将 AZ400K 显影液与去离子水按照 1∶3 的体积比进行混合，配制成稀释了的显影液，再将 UV 曝光后的基片放在该显影液中显影，显影时间根据曝光情况调整，从显影液中取出样品并用去离子水清洗干净后用氮气吹干便可获得最终的实验样品。本实验使用 Leica Microsystems DM8000M 光学显微镜对所获得的样品进行表征。

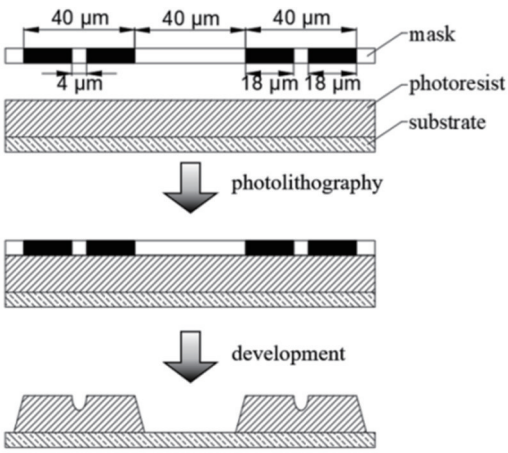

图 2 光刻工艺示意图

Fig. 2 Schematic diagram of photolithography process

3 实验结果分析与讨论

本实验所制备的微米级单凹字型双层复合结构的平面和截面显微镜照片分别如图 3(a)～(c)所示，使用的是图 1(a)所示的 1 号掩模版。图 3(a)所示样品的曝光能量为 128 mJ/cm^2，显影时间为 700 s，所制备的单凹字型双层复合结构的中央凹形缺口深度为 4.86 μm，达到光刻胶总厚度的 60.75%。假设在中央凹形缺口的最低处存在一条水平线，将该水平线以上的部分看作一层微米结构，将该水平线以下的部分看作另一层微米结构，则该中央凹形缺口的存在成功地将原来的微米级单层结构分成了微米级双层复合结构。这样的一个微米级双层复合结构以往在传统光刻技术中只能利用套刻工艺来实现，而套刻工艺的对准过程极其复杂，故制备此类结构的难度相当高。然而，利用一步光刻技术制备微米级双层复合结构工艺很简单。

图 3(b)所示样品的曝光能量为 138 mJ/cm^2，显影时间为 700 s，所制备的单凹字型双层复合结构的中央凹形缺口的深度为 5.96 μm，达到光刻胶总厚度的 74.5%。图 3(c)所示样品的曝光能量为 240 mJ/cm^2，显影时间为 410 s，中央凹形缺口处的光刻胶已经显影到基片表面上，无任何残留光刻胶，其结构深度与光刻胶厚度相同(均为 8 μm)，此时得到左右两个类梯形分立结构。基本规律是曝光能量越大，所获得的中央凹形缺口的深度越大。当曝光能量足够大时，中央凹形

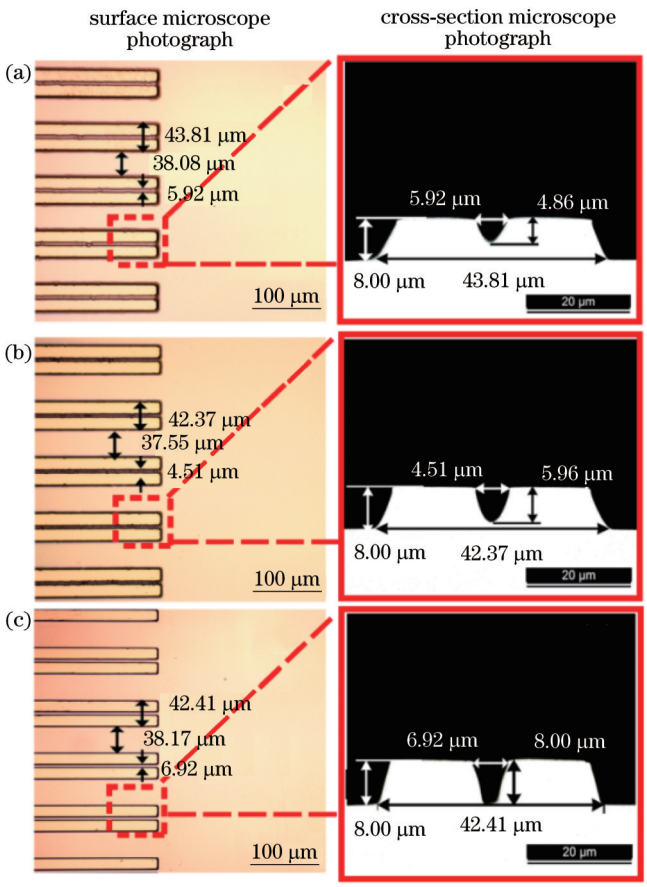

图 3 不同曝光能量和显影时间下单凹字型双层复合结构样品的平面图和截面图。(a)曝光能量为 128 mJ/cm^2，显影时间为 700 s；(b)曝光能量为 138 mJ/cm^2，显影时间为 700 s；(c)曝光能量为 240 mJ/cm^2，显影时间为 410 s

Fig. 3 Surface and cross-section images of single-concave-type double-layer composite structure sample under different exposure energies and development times. (a) Exposure energy of 128 mJ/cm^2 and development time of 700 s; (b) exposure energy of 138 mJ/cm^2 and development time of 700 s; (c) exposure energy of 240 mJ/cm^2 and development time of 410 s

缺口处的光刻胶显影后无任何残留，此时微米级双层复合结构消失了，在基片上得到两个微米尺寸的类梯形分立结构。

为了更加全面地掌握该技术，进一步开展了微米级双凹字型双层复合结构的实验工作，使用的是图 1(b)所示的 2 号掩模版。所制备的微米级双凹字型双层复合结构的平面和截面显微镜照片如图 4(a)～(c)所示。图 4(a)所示样品的曝光能量为 125 mJ/cm^2，显影时间为 750 s，该双凹字型双层复合结构的凹形缺口深度为 3.56 μm，为光刻胶总厚度的 44.5%。图 4(b)所示样品的曝光能量为 130 mJ/cm^2，显影时间为 750 s，该双凹字型双层复合结构的凹形缺口深度为 5.82 μm，为光刻胶总厚度的 72.75%。图 4(c)所示样品的曝光能量为 160 mJ/cm^2，显影时间为 750 s，该双凹字型双层复合结构的凹形缺口深度为 7.96 μm，达到光刻胶总厚度的 99.5%，此时凹形缺口处的基片并未完全裸露出来。实验结果表明：在相同的显影条件下，通过控制曝光能量的大小，可以实现凹形缺口深度的控制。不均匀的曝光条件或显影工艺的些许差别都可能会造成左右两侧凹形缺口深度不完全一致的现象出现。对 8 μm 厚的 AZ9260 光刻胶来说，可以认为 160 mJ/cm^{2}的曝光能量是凹形缺口处的玻璃基片能否裸露出来的能量阈值：当曝光能量不大于 160 mJ/cm^{2}时，才可以制备出微米级双层复合结构；当曝光能量大于 160 mJ/cm^{2}时，会制备出微米级单层分立结构。

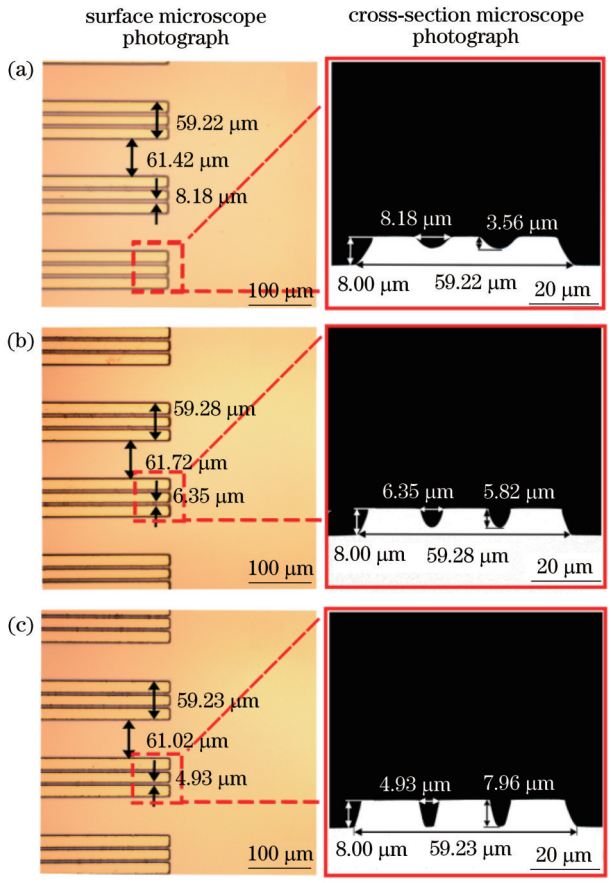

图 4 不同曝光能量和相同显影时间下双凹字型双层复合结构样品的平面图和截面图。(a)曝光能量为 125 mJ/cm^2，显影时间为 750 s；(b)曝光能量为 130 mJ/cm^2，显影时间为 750 s；(c)曝光能量为 160 mJ/cm^2，显影时间为 750 s

Fig. 4 Surface and cross-section images of double-concave-type double-layer composite structure sample under different exposure energies and identical development time. (a) Exposure energy of 125 mJ/cm^2 and development time of 750 s; (b) exposure energy of 130 mJ/cm^2 and development time of 750 s; (c) exposure energy of 160 mJ/cm^2 and development time of 750 s

4 理论分析

分析样品制备工艺很容易看出 UV 曝光和显影这

两步实验工艺中隐藏着产生第3章所示的实验结果的原因。采用有限差分时域法对1号掩模版曝光时光刻胶表面(z=0)、光刻胶表面下方4 μm(z=4 μm)和光刻胶表面下方8 μm(z=8 μm)处的光场情况进行了仿真分析。建立Cr掩模版的数值仿真模型,仿真模型的yz面示意图如图5所示。选取一个周期作为仿真单元,仿真模型结构参数的相关数据如图1(a)所示,80 μm周期宽度沿y方向满足周期性边界条件。设曝光光源发出平面波且均匀地入射到Cr掩模版上,曝光波长为365 nm。规定z方向沿平面波传播方向且满足完美匹配层(PML)边界条件(BC),x方向垂直于纸面向里并设置宽度为1 μm,满足周期性边界条件,并设定Cr膜的厚度为100 nm。假设光刻胶的折射率数值不随曝光过程发生任何变化,不考虑光刻胶对光的吸收,并将光刻胶的折射率设为1.67,光刻胶层的厚度设定为8 μm。根据图3和图4中的实验结果,只有当光刻胶曝光能量不足时,才能形成微米级双层复合结构。当曝光能量不足时,认为光波传播到基片表面时与基片的相互作用已经很弱,故在本文的仿真模型中不再考虑光传播到基片表面反射时对光刻胶内光场分布的影响。

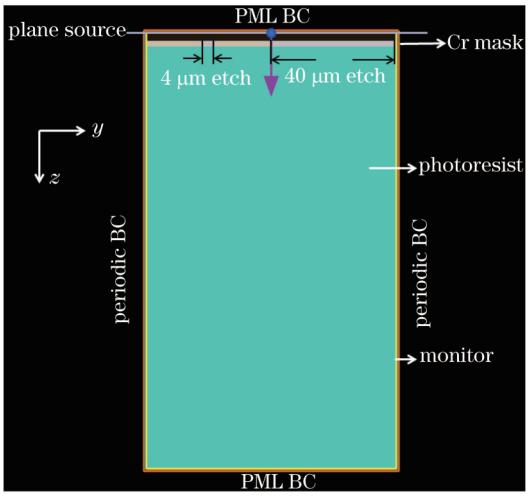

图5 仿真模型的yz面示意图

Fig. 5 Schematic diagram of yz plane of simulation model

图6是图5所示仿真模型的光强分布仿真结果。从图6(a)可以看到整个8 μm光刻胶层中的光强分布情况:4 μm窄缝正下方的光强分布随着光刻胶厚度的增加而变窄,这是由光在光刻胶内部衍射造成的,此时光的能量也发生了向外扩散,并不能够被完全限制在4 μm窄缝正下方的光刻胶内传播;40 μm宽缝下方光强分布随着光刻胶厚度的增加并未发生特别明显的变化。从图6(b)可以看到,在光刻胶表面(z=0)处,40 μm宽缝的内部光强较为均匀,但越靠近边缘光强波动越大,边界处光强突然增大,而4 μm窄缝因宽度较窄在整个缝宽范围内光强的波动均较大,且边界处波动与40 μm宽缝波动幅度一致,这说明4 μm窄缝和40 μm宽缝在边界处产生了明显的衍射效应,而这一现象在文献[24]中已得到详细解释。图6(c)、(d)分别展示了光刻胶表面下方4 μm(z=4 μm)和8 μm(z=8 μm)处的光场分布情况。可以看出:随着光刻胶厚度的增加,在整个缝宽范围内4 μm窄缝中的光强波动越来越剧烈,剧烈的光强波动会导致光刻胶在曝光时的反应效率降低;40 μm宽缝边缘部分的剧烈波动范围虽然也在逐渐向中心移动,但其内部很宽的范围内始终保持着均匀的光强分布,这保证了光刻胶在曝光时能够发生连续不断的光化学反应。在曝光能量不足的情况下,这样的光强波动和分布情况最终导致了4 μm窄缝下方的光刻胶的曝光效率低于40 μm宽缝。也就是说,在同时曝光的情况下,当40 μm宽缝下方的光刻胶已完全反应完毕时,4 μm窄缝下方的光刻胶还会剩余部分未反应的光刻胶,显影后便会产生微米级双层复合结构。

在实际的曝光过程中,光刻胶对光能量总存在一定的吸收,故光强会在传播方向上缓慢减小,从而将引起光刻胶上部曝光过度而下部曝光不足,最终导致显影后图形的顶部线宽大于底部线宽,如图3和图4中样品的截面图所示。底部的不平整是由曝光过程中光场衍射使光刻胶经过光化学反应后产生的光敏化合物不均匀分布造成的[25]。对于正性光刻胶,曝光过程进行得越彻底,其光敏化合物的含量就越低,显影速率就越快,反之则显影速率就越慢。对于厚层光刻胶,当曝光能量不足时,随着显影时间和显影深度的增加,4 μm窄缝中的显影液更新速度跟不上40 μm宽缝中显影液的更新速度将进一步促使显影后形成微米级双层复合结构。

5 结 论

提出了一种利用一步光刻技术制备微米级双层复合结构的方法,展示了两种光刻掩模版的图案结构参数,并使用这两种掩模版进行了实验探索。实验结果表明:与常规的套刻工艺相比,利用该技术能够非常简单地构建出微米级双层复合结构,8 μm厚的AZ9260光刻胶的曝光能量阈值约为160 mJ/cm^2。利用有限差分时域法分析了光刻曝光时掩模版后的光场分布情况。仿真结果表明:随着光刻胶厚度的增加,4 μm窄缝的整个缝宽范围内光强波动越来越剧烈,剧烈的光强波动降低了光刻胶在曝光时的反应效率,最终导致同时曝光时4 μm窄缝下的光刻胶所接收到的曝光能量比40 μm宽缝下的光刻胶少,这也是微米级双层复合结构能够通过一步光刻技术制备出来的根本原因。4 μm窄缝中的显影液更新速度跟不上40 μm宽缝中显影液的更新速度将进一步促使微米级双层复合结构的形成。在进行掩膜光刻时,掩模版上宽透光区域下的光刻胶将比窄透光区域下的光刻胶更快地显影到基片上。根据这一规律,可以设计出各种不同的掩模版,

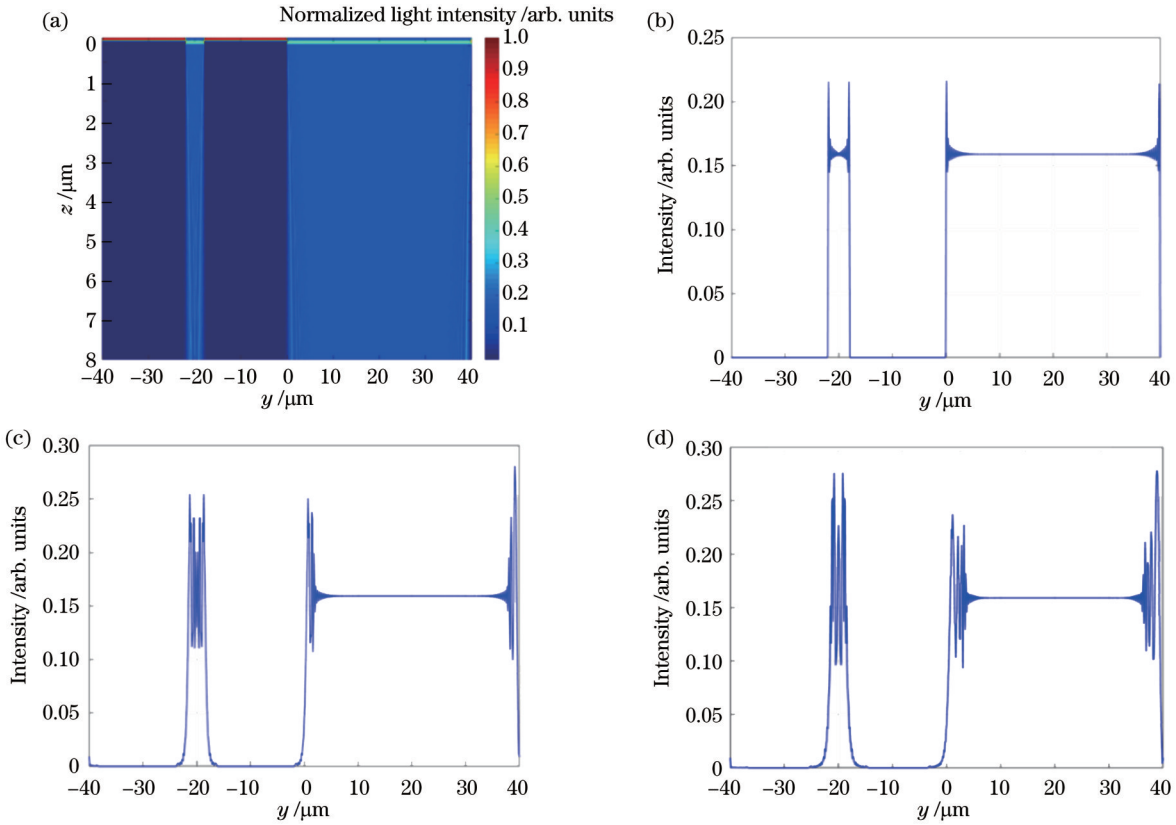

图 6 光强分布仿真结果。(a) yz 面光强的整体分布情况；(b) $z=0$ 处的光强分布曲线；(c) $z=4$ μm 处的光强分布曲线；(d) $z=8$ μm 处的光强分布曲线

Fig. 6 Simulation results of light intensity distribution. (a) Overall distribution of light intensity on yz plane; (b) light intensity distribution curve at $z=0$; (c) light intensity distribution curve at $z=4$ μm; (d) light intensity distribution curve at $z=8$ μm

利用一步光刻技术有望制备出各种各样的微米级双层复合结构甚至微米级多层复合结构。本研究所展示的掩模版对制备各种微米级多层复合结构均具有参考意义。

参 考 文 献

[1] Bhushan B, Jung Y C, Nosonovsky M. Lotus effect: surfaces with roughness-induced superhydrophobicity, self-cleaning, and low adhesion[M]//Bhushan B. Springer handbook of nanotechnology. Springer handbooks. Heidelberg: Springer, 2010: 1437-1524.

[2] Gao X F, Yan X, Yao X, et al. The dry-style antifogging properties of mosquito compound eyes and artificial analogues prepared by soft lithography[J]. Advanced Materials, 2007, 19(17): 2213-2217.

[3] Luo Y H, Liu Y F, Zhang D Y, et al. Influence of morphology for drag reduction effect of sharkskin surface[J]. Journal of Mechanics in Medicine and Biology, 2014, 14(2): 1450029.

[4] Luo Y H, Yuan L, Li J H, et al. Boundary layer drag reduction research hypotheses derived from bio-inspired surface and recent advanced applications[J]. Micron, 2015, 79: 59-73.

[5] Liu K S, Du J X, Wu J T, et al. Superhydrophobic gecko feet with high adhesive forces towards water and their bio-inspired materials[J]. Nanoscale, 2012, 4(3): 768-772.

[6] Tang Q T, Yao H Y, Xu B B, et al. Integrated effect of hierarchical structure combining isotropic worm-like pit with anisotropic inverted nanopyramid for quasi-omnidirectional c-Si solar cell[J]. Materials Science in Semiconductor Processing, 2021, 121: 105363.

[7] Nowduri B, Schulte S, Decker D, et al. Biomimetic nanostructures fabricated by nanoimprint lithography for improved cell-coupling[J]. Advanced Functional Materials, 2020, 30(45): 2004227.

[8] Yang M Y, Xu K, Wang L. Flexible touch sensor fabricated by double-sided nanoimprint lithography metal transfer[J]. Nanotechnology, 2020, 31(31): 315302.

[9] Zhang J, Ye S B, Liu H L, et al. 3D printed piezoelectric BNNTs nanocomposites with tunable interface and microarchitectures for self-powered conformal sensors[J]. Nano Energy, 2020, 77: 105300.

[10] Jambhulkar S, Xu W H, Franklin R, et al. Integrating 3D printing and self-assembly for layered polymer/nanoparticle microstructures as high-performance sensors[J]. Journal of Materials Chemistry C, 2020, 8(28): 9495-9501.

[11] Oladapo B I, Zahedi S A, Ismail S O, et al. 3D printing of PEEK-cHAp scaffold for medical bone implant[J]. Bio-Design and Manufacturing, 2021, 4(1): 44-59.

[12] Rad M R, Fahimipour F, Dashtimoghadam E, et al. Osteogenic differentiation of adipose-derived mesenchymal stem cells using 3D-Printed PDLLA/β-TCP nanocomposite scaffolds[J]. Bioprinting, 2021, 21: e00117.

[13] Wang T, Yu W, Li C, et al. Biomimetic compound eye with a high numerical aperture and anti-reflective nanostructures on curved surfaces[J]. Optics Letters, 2012, 37(12): 2397-2399.

[14] 高文, 郑美玲, 金峰, 等. 飞秒激光快速制备大面积二维微纳结构[J]. 激光与光电子学进展, 2020, 57(11): 111421.
Gao W, Zheng M L, Jin F, et al. Fast fabrication of large-area two-dimensional micro/nanostructure by femtosecond laser[J]. Laser & Optoelectronics Progress, 2020, 57(11): 111421.

[15] Wang Z, Nandyala D, Colosqui C E, et al. Glass surface micromachining with simultaneous nanomaterial deposition by picosecond laser for wettability control[J]. Applied Surface Science, 2021, 546: 149050.

[16] 王成. 微纳复合多级结构的可控制造方法及摩擦发电性能研究[D]. 西安: 西安理工大学, 2020: 11-24.
Wang C. Research on controllable manufacturing method and triboelectric performance of micro-nano composite multistage structure[D]. Xi'an: Xi'an University of Technology, 2020: 11-24.

[17] Chen X L, Xiong J Q, Parida K, et al. Transparent and stretchable bimodal triboelectric nanogenerators with hierarchical micro-nanostructures for mechanical and water energy harvesting [J]. Nano Energy, 2019, 64: 103904.

[18] Lü T, Cheng Z J, Zhang D J, et al. Superhydrophobic surface with shape memory micro/nanostructure and its application in rewritable chip for droplet storage[J]. ACS Nano, 2016, 10(10): 9379-9386.

[19] 陈国栋, 张子南, 李思坤, 等. 深紫外计算光刻技术研究[J]. 激光与光电子学进展, 2022, 59(9): 0922007.
Chen G D, Zhang Z N, Li S K, et al. Study on deep ultraviolet computational lithography techniques[J]. Laser & Optoelectronics Progress, 2022, 59(9): 0922007.

[20] 张子南, 李思坤, 王向朝, 等. 极紫外光刻快速掩模优化方法[J]. 光学学报, 2022, 42(13): 1305002.
Zhang Z N, Li S K, Wang X Z, et al. Fast mask optimization method for extreme ultraviolet lithography[J]. Acta Optica Sinica, 2022, 42(13): 1305002.

[21] 张子南, 李思坤, 王向朝. EUV 光刻三维掩模成像研究进展[J]. 激光与光电子学进展, 2022, 59(9): 0922021.
Zhang Z N, Li S K, Wang X Z. Research progress on the imaging of three-dimensional mask for extreme ultraviolet lithography[J]. Laser & Optoelectronics Progress, 2022, 59(9): 0922021.

[22] 马旭, 张胜恩, 潘毅华, 等. 计算光刻研究及进展[J]. 激光与光电子学进展, 2022, 59(9): 0922008.
Ma X, Zhang S E, Pan Y H, et al. Research and progress of computational lithography[J]. Laser & Optoelectronics Progress, 2022, 59(9): 0922008.

[23] Zhang D Y, Xing W Q, Li W R, et al. Fabrication of multiple parallel microchannels in a single microgroove via the heating assisted MIMIC technique[J]. Micromachines, 2022, 13(3): 364.

[24] 李木军. 接近式光刻仿真研究[D]. 合肥: 中国科学技术大学, 2007: 52-57.
Li M J. Research on simulation of proximity UV-lithography[D]. Hefei: University of Science and Technology of China, 2007: 52-57.

[25] 唐雄贵. 厚胶光学光刻技术研究[D]. 成都: 四川大学, 2006: 90-102.
Tang X G. Research on optical lithography of thick film resists [D]. Chengdu: Sichuan University, 2006: 90-102.

One-Step Photolithographic Preparation Technology of Micron-Level Double-Layer Composite Structures

Zhang Dengying[1,2,3,4*], Zhu Linwei[3], Li Weiren[3], Gao Honghu[3], Xing Wenqiang[3], Jiang Xiaotong[3], Wang Jun[2], Xu Zheng[1,4**]

[1]*Institute of Optoelectronics Technology, Beijing Jiaotong University, Beijing* 100044, *China*;

[2]*Beijing Solar Power Research Institute Co., Ltd., Beijing* 101102, *China*;

[3]*School of Physics and Optoelectronic Engineering, Ludong University, Yantai* 264025, *Shandong, China*;

[4]*Key Laboratory of Luminescence and Optical Information, Ministry of Education, Beijing Jiaotong University, Beijing* 100044, *China*

Abstract

Objective In bionics research, micron-level double-layer composite structures can usually show better mechanical, optical, and chemical properties than single-layer structures. Designing and constructing these unique biomimetic microstructure surfaces for human use is a hot research topic in recent years. The traditional photolithography technology is very convenient and has the advantage of simple process when it is applied to prepare the micron-level single-layer structures. However, when the traditional photolithography technology is adopted to prepare the micron-level double-layer composite structures, it needs to use the overlay lithography process for many times, which will greatly increase the manufacturing difficulty and processing cost of the microstructure. To overcome the above difficulties, researchers have developed a variety of microstructure processing methods, such as dry/wet etching, nanoimprinting, 3D printing, self-assembly, laser processing, photolithography, replication molding, and electrospinning. A variety of single-layer microstructure surfaces can be prepared by using these technology combinations, and even multi-scale micron-level composite structure surfaces can be prepared. However, the combinations often lead to more cumbersome processing procedures and higher costs of micron-level composite structures. To solve these problems, a method to adjust the exposure efficiency of photoresist by changing the width of the light transmitting part on the mask is proposed. By this method, the micron-level double-layer composite structures can be obtained on the positive photoresist with only one exposure and one development, which greatly reduces the processing difficulty and manufacturing costs of such structures

and provides a new strategy for fabricating multi-scale micron-level composite structures.

Methods Two lithographic masks with different parameters are designed and purchased from the 55th Research Institute of China Electronics Technology Group Corporation. The pattern of the mask and the schematic diagram of the photolithography process are shown in Fig. 1 and Fig. 2, respectively. The specific experimental process is detailed as follows. The K_9 glass substrate is cleaned by an ultrasonic cleaner in acetone, ethanol, and deionized water for 5 min each and then dried with nitrogen flow. The AZ9260 photoresist film with a thickness of 8 μm is spin-coated on a 5.08-cm K_9 substrate at 2500 r/min for 40 s using Laurell WS-650Mz spin coater. After standing at room temperature for 10 min, the substrate is placed on a 65 ℃ hot plate for 5 min, a 95 ℃ hot plate for 10 min and a 110 ℃ hot plate for 5 min, and finally cooled to room temperature. The ultraviolet (UV) lithographic exposure process is performed on Midas MDA-400M. The exposure energy of different samples is set between 125 mJ/cm^2 and 240 mJ/cm^2. The photoresist development is carried out with AZ400K developer (the volume ratio of AZ400K developer to deionised water is 1∶3) after UV exposure. Leica Microsystems DM8000M optical microscope is used to characterize the obtained samples. In addition, the light field distribution during mask exposure is analyzed by the finite-difference time-domain method to find out the formation mechanism of the micron-level double-layer composite structures.

Results and Discussions Two kinds of micron-level double-layer composite structures fabricated by one-step photolithographic preparation technology are presented (Fig. 3 and Fig. 4). The experimental results show that the depth of the concave notch can be effectively controlled by adjusting the exposure energy. The basic rule is that as the exposure energy becomes larger, the depth of the concave notch will be greater. When the exposure energy is large enough, there is no residual photoresist at the central concave notch after development. At this time, the micron-level double-layer composite structure disappears, and two micron-size discrete structures are obtained on the substrate (Fig. 3). The influence of exposure energy on the depth of the concave notch is studied with identical development time (Fig. 4). For 8 μm thick AZ9260 photoresist film, the exposure energy not higher than 160 mJ/cm^2 is the key to preparing the micron-level double-layer composite structures (Fig. 4). Schematic diagram of *yz* plane of the simulation model is demonstrated (Fig. 5). The light field distribution behind the mask during lithography exposure is analyzed by the finite-difference time-domain method (Fig. 6). The simulation results show that the exposure efficiency of the photoresist under 4 μm narrow slit is lower than that under 40 μm wide slit, which is the fundamental reason why the micron-level double-layer composite structures can be prepared by one-step lithography technology.

Conclusions The application of the one-step photolithographic preparation technique proposed in this paper can effectively reduce the difficulty in fabricating micron-level double-layer composite structures. The experimental results show that the fabrication process of the micron-level double-layer composite structures using the proposed method is very simple compared with that using overlay lithography technology, and only one exposure and one development process are needed. The maximum exposure energy of 8 μm thick AZ9260 photoresist should not be higher than 160 mJ/cm^2 to obtain micro-level double-layer composite structures. The light field distribution behind the mask during lithography exposure is analyzed by the finite-difference time-domain method. The simulation results show that the exposure efficiency of the photoresist under 4 μm narrow slit is lower than that under 40 μm wide slit, which is also the fundamental reason why the micron-level double-layer composite structures can be prepared by one-step lithography technology. The developer renewal speed in the 4 μm narrow slit is less than that in the 40 μm wide slit, further promoting the formation of the micron-level double-layer composite structures. During the mask lithography, the photoresist under the wide light transmitting area on the mask will be developed to the substrate faster than that under the narrow light transmitting area. According to this rule, various masks can be designed, and it is expected to prepare a variety of micron-level double-layer composite structures or even micron-level multi-layer composite structures by this method. The masks shown in this paper have reference significance for preparing various micron-level multi-layer composite structures.

Key words optical devices; microstructure fabrication; photolithography; micron-level double-layer composite structures; finite-difference time-domain method